Chemical Geology 530 (2019) 119331

Contents lists available at ScienceDirect

Chemical Geology

journal homepage: www.elsevier.com/locate/chemgeo

Calcium carbonate precipitation mediated by bacterial carbonic anhydrase in a karst cave: Crystal morphology and stable isotopic fractionation

Xianfu Lü[a,b,c], Qiufang He[c,*], Zhijun Wang[d], Min Cao[c], Jingyao Zhao[e], Jianjian Jiang[c], Ruiyi Zhao[f], Hong Zhang[c]

[a] Key Laboratory of Tibetan Environment Changes and Land Surface Processes, Institute of Tibetan Plateau Research, Chinese Academy of Sciences, Beijing 100101, China
[b] University of Chinese Academy of Sciences, Beijing 100101, China
[c] School of Geographical Sciences, Southwest University, Chongqing Key Laboratory of Karst Environment, Chongqing, 400715, China
[d] Key Laboratory of Karst Dynamics, MLR & Guangxi, Institute of Karst Geology, Chinese Academy of Geological Sciences, Guilin 541004, China
[e] Institute of Global Environment Change, Xi'an Jiaotong University, Xi'an, 710054, China
[f] College of Architecture and Urban Planning, Chongqing Jiaotong University, Chongqing 400074, China

ARTICLE INFO

Editor: Hailiang Dong

Keywords:
Modern speleothem
Microbially induced carbonate precipitation (MICP)
Lysinibacillus
Extracellular carbonic anhydrase (CAex)
Isotope fractionation

ABSTRACT

Stable oxygen ($\delta^{18}O$) and carbon ($\delta^{13}C$) isotopes of speleothems are widely used as important proxies for paleoclimatic and paleoenvironment reconstructions. However, the influence of microbial activity on carbon and oxygen isotope fractionation during speleothem precipitation remains unclear. Bacterial carbonic anhydrase (CA) can promote calcium carbonate precipitation to catalyze the mutual transformation between CO_2 and HCO_3-. CA-producing bacteria (*Lysinibacillus sp.* strain LHXY2) were separated in the Xueyu Cave, Chongqing, SW China, and used in laboratory and cave in situ models to investigate their influence on the precipitation amount, mineral components, crystal morphology and carbon and oxygen isotope fractionation of $CaCO_3$. A CA activity gradient was applied in the laboratory model by considering various CA inhibitor acetazolamide (AZ) concentrations, which showed that the CA activity could substantially enhance precipitation, alter the mineral components and morphology, and reduce the $\delta^{13}C$ and $\delta^{18}O$ values of the $CaCO_3$ formed. Most importantly, the laboratory and in situ model results revealed approximately -7‰ and -1.4‰ $\delta^{13}C$ shifts, respectively, compared to the bacteria-free model results, which indicated that microbial-driven carbon isotopic fractionation can cause great uncertainties in paleoclimate and paleoenvironment reconstructions.

1. Introduction

Speleothems (e.g., stalagmites and stalactites) are important archives for climate change reconstruction (Wang et al., 2001; Yuan et al., 2004). The stable oxygen and carbon isotope compositions ($\delta^{18}O$ and $\delta^{13}C$, respectively) of speleothems are widely used as invaluable proxies of paleoclimates and paleoenvironments (Cheng et al., 2016; Zhang et al., 2018). In particular, the $\delta^{18}O$ values of stalagmites have been successfully used to reconstruct paleoclimate changes during the past 640 ka (Cheng et al., 2016; Wang et al., 2001, 2005; 2008). Compared with speleothem $\delta^{18}O$ values, the interpretation of speleothem $\delta^{13}C$ values is more challenging since carbon isotope fractionation within karst systems is more complicated (Dredge et al., 2013; Fohlmeister et al., 2018; Hansen et al., 2017; Kele et al., 2015; Versteegh et al., 2017). In general, the carbon isotopes of a speleothem can be affected by changes in the atmospheric CO_2 concentration, vegetation cover and soil CO_2, changes in CO_2 solubility leading to the dissolution of calcium carbonate, water-rock interactions, prior calcite precipitation, and carbon isotope fractionation during the process of calcite precipitation within the cave (Li et al., 1997). In addition, the carbon isotope composition and fractionation of speleothems are affected by the redissolution and redeposition process equilibrium, the temperature and humidity of the cave (thermodynamic equilibrium fractionation), the height and rate of drip water (kinetic disequilibrium fractionation), the degree of mineral recrystallization (mainly the transformation of aragonite to calcite) and biological activities (Li et al., 2011b). Therefore, there are still uncertainties in the accurate interpretation of speleothem $\delta^{13}C$ values for paleoenvironmental reconstruction.

The influence of microorganisms on speleothem precipitation has attracted considerable attention (Portillo and Gonzalez, 2011; Rusznyak et al., 2011). Studies on cave microbes have focused on, for instance, bacterial community and nutrient cycling (Engel et al., 2010;

* Corresponding author.
E-mail address: hqfeddy@swu.edu.cn (Q. He).

https://doi.org/10.1016/j.chemgeo.2019.119331
Received 19 February 2019; Received in revised form 22 September 2019; Accepted 4 October 2019
Available online 14 October 2019
0009-2541/

Kimble et al., 2018; Ortiz et al., 2014; Tebo et al., 2015), the process of microbially induced carbonate precipitation (MICP) (Okyay and Rodrigues, 2015), and the role of microbial activities on speleothem precipitation (Dhami et al., 2018; Kondratyeva et al., 2016; Maciejewska et al., 2017; Zhuang et al., 2018). However, the effect of microbial processes on speleothem isotope geochemistry has not been investigated in great detail. Only a few studies have investigated carbon isotope fractionation during precipitation in microbially mediated speleothems (Sanchez-Moral et al., 2012).

Almost all microorganisms can induce calcium carbonate precipitation under specific conditions (Boquet et al., 1973), which alter the hydrochemical conditions, such as the pH and CO_3^{2-} concentration, through metabolic activities (Riding, 2006) and secreted extracellular polymeric substances (López-Moreno et al., 2014; Sánchez-Román et al., 2015) that participate in the calcium carbonate precipitation process. In particular, carbonic anhydrase (CA, EC 4.2.1.1) (Jimenez-Lopez et al., 2003; Tran et al., 2013) plays an important role in calcium carbonate precipitation. CA catalyzes the mutual transformation between CO_2 and HCO_3-, which is commonly present in eukaryotes and prokaryotes (Smith and Ferry, 2000), such as bovine erythrocytes (Power et al., 2016; Power et al., 2013), algae (Kanth et al., 2012; Swarnalatha et al., 2015) and bacteria (Kim et al., 2012) and is considered one of the key enzymes promoting carbonate mineralization. However, the effects of CA on isotopic fractionation during speleothem precipitation remain unclear. The disequilibrium fractionation effect of $\delta^{18}O$ in regard to biogenic carbonates renders the accurate interpretation of paleo-oceanographic records impossible (Uchikawa and Zeebe, 2012). Compared with oxygen isotopes, the research on the CA effect on carbon isotope fractionation during calcium carbonate precipitation is relatively insufficient (Millo et al., 2012a; Millo et al., 2012b). Acetazolamide (AZ) is a specific inhibitor of extracellular CA (CAex) (Moulin et al., 2011); thus, the effect of algal CAex on carbon isotope fractionation can be studied using bacterial cultures with or without the addition of AZ (Wu et al., 2012). To address this critical question, a CA-producing bacterium was separated from the surface of the modern speleothem in the Xueyu Cave and then injected into both laboratory and cave in situ models to examine the effects of CA on the carbon isotope composition of calcite. A CA activity gradient was applied with various CA inhibitor concentrations to study the promoting effect of CA. We hypothesized that the CA activity could substantially enhance precipitation, alter the mineral components and crystal morphology, and lead to carbon and oxygen isotope fractionation during calcite precipitation. We attempted to provide insights into the mechanism and isotope composition of calcium carbonate under the action of microbial CA and a scientific basis for elucidating the deviations caused by microbial activities in paleoclimate and paleoenvironment reconstructions.

2. Materials and methods

2.1. Sampling sites

The Xueyu Cave (29°47′00″ N; 107°47′13″ E; altitude of 233 m) is located in the lower reach of the Long River, a tributary of the Yangtze River, approximately 12 km southeast of Fengdu County, Chongqing Municipality, SW China (Fig. 1a), which is developed in Lower Triassic limestones (T1j). The overburden of the cave consists of a 150–250 m thick limestone layer with well-vegetated evergreen broadleaf woods. A perennial subterranean stream has developed through the limestone (Fig. 1b), the catchment of which is approximately 8-9 km^2. The stream outlet is also the only known entrance of the cave. The regional climate is dominated by the Asian monsoon climate, with a multiannual precipitation of 1072 mm and a temperature of 17.5 ℃ and is characterized by cold and dry winters from November to April and hot and rainy summers from May to October with 70% of the annual rainfall. The inner part of the Xueyu Cave, which is 300 m away from the entrance has an air temperature ranging from 16.8℃ to 19.1℃. The modern speleothem precipitation rate is approximately 295 mg/yr. (glass sheets that are 9 cm in diameter) with a rare snow-white jade-like presentation (Fig. 1d).

Sterilized swabs were used to collect bacteria from the surface of the modern speleothems below active drip waters (Fig. 1c), including stalagmites, soda straws and stalactites and stored in sterilized centrifuge tubes at 4 ~ 8 ℃ until separation.

2.2. Separation, purification and identification of Lysinibacillus sp. LHXY2

The bacteria were screened, separated and purified using the B-4 solid medium (2.5 g/L calcium acetate, 4.0 g/L yeast extract, 15.0 g/L agar, and a pH of 8.0), TSA medium (15 g/L tryptone, 5 g/L soybean peptone, 5 g/L NaCl, 15 g/L agar, and a pH of 7.1–7.4), and B-4 liquid medium (2.5 g/L calcium acetate and 4.0 g/L yeast extract, with a pH of 8.0). Bacterial DNA was extracted using the Biospin Bacterial Genomic DNA Extraction Kit (BioFlux) following the standard protocol, and the DNA extraction was preserved at -20 ℃. The 16S rDNA gene was amplified using primers 27 F (5'-AACTGAAGAGTTTGATCCTGGCTC-3') and 1492R (5'-TACGGTTACCT TGTTACGACTT-3') and visualized by electrophoresis on 1% agarose gel. The positive polymerase chain reaction (PCR) products were sequenced following Sanger's method as suggested by Sangon Biotechnology. The 16S rDNA gene sequences were stored in the NCBI nonredundant (NCBI-nr) database with an accession number (accession no. MF773945). Strain LHXY2 was identified as *Lysinibacillus* sp. LHXY2.

2.3. Laboratory calcium carbonate precipitation experiments

In the laboratory, the B-4 liquid medium was added to a 250 mL conical flask, and the CAex enzyme inhibitor acetazolamide (AZ) was added to modify the gradient CA activities. The final AZ concentrations of the 50 mL culture solutions were 0 mmol/L, 0.5 mmol/L, 1 mmol/L, 2 mmol/L, 4 mmol/L and 8 mmol/L by adding a certain volume of the 20 mmol/L AZ solution (Table 1). Thereafter, 1 mL incubation of *Lysinibacillus* sp. LHXY2 was added to each culture solution and incubated in darkness at 28 ℃ for 18 d.

Each treatment was prepared in triplicate with a sterilized control (without incubation injection) and a blank control (without incubation injection and AZ). After 18 d of incubation, all cultures were filtrated and analyzed to determine the calcium concentration and pH value of the filtrates, while the precipitates were dried at 40 ℃ to measure the amount and analyze the mineral components, crystal morphology and $\delta^{13}C$ and $\delta^{18}O$ values.

2.4. Cave in situ experiments

The cave in situ experiments were conducted using glass columns filled with glass beads (1 mm in diameter, 240 g). An arched glass sheet was used to collect calcium carbonate. Glass fibers were placed on the top and bottom layers to prevent the glass beads from being washed away by the cave drip water. The top and bottom layers of each simulation equipment contained 3 g glass fibers, and the middle layer contained 240 g glass beads. The top and bottom of the simulation equipment were uncovered to expose the incubation devices to the cave environment (Fig. 2). Before being placed at the monitoring sites, the simulation columns were assembled in the laboratory, sterilized for 20 minutes at 121℃, and then transported to the Xueyu Cave in an aseptic storage box. The simulation equipment was placed at three drip monitoring sites (D1) with similar drip rates and overburdens.

Three treatments were designed to monitor the cave in situ precipitation process. In treatment 1, the single-bacterium (*Lysinibacillus* sp. LHXY2) incubation containing AZ (LHXY2 + 25 mL AZ) was added consecutive times (25 mL of 10 mmol/L AZ in total). Treatment 2 included the single-bacterium (*Lysinibacillus* sp. LHXY2) incubation containing no AZ in three additions (15 mL in total, and 5 mL each time). Treatment 3 contained three additions of mixed-strain incubations (XYQE, XY31 and XYLG, which induced the maximum amount of

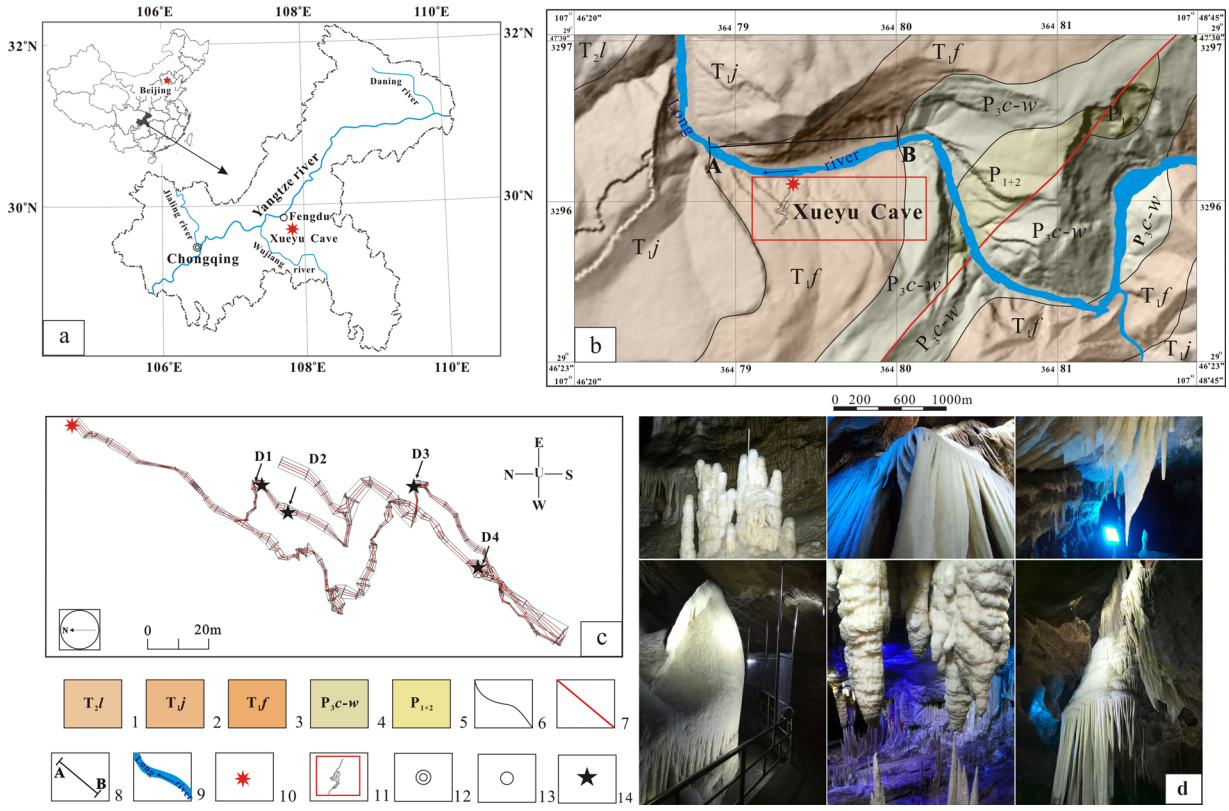

Fig. 1. Location, geological setting, sampling sites and speleothems of the Xueyu Cave. **a.** Location of the Xueyu Cave; **b.** geological setting of the Xueyu Cave; **c.** morphology of the Xueyu Cave; D1, D2, D3 and D4 are the drip water monitoring sites; **d.** stalagmites, flowstones, cave flags, cave shield, stalactites and stone curtain; (1) Middle Triassic Leikoupo Formation, (2) Lower Triassic Jialingjiang Formation, (3) Lower Triassic Feixianguan Formation, (4) Upper Permian series, (5) Lower Permian series, (6) conformity stratigraphic boundary, (7) fault, (8) location of the measured geological section, (9) river/stream and name, (10) location of the cave mouth, (11) the Xueyu Cave, (12) bacteria and drip water sampling sites, (13) city, and (14) county.

Table 1
Calcium carbonate precipitation treatment in the laboratory experiments.

Treatment	B-4 liquid medium (mL)	AZ (mL)	Medium concentration (mmol/L)	Bacteria (mL)
1	50	0	0	1
2	48.75	1.25	0.5	1
3	47.5	2.5	1	1
4	45	5	2	1
5	40	10	4	1
6	30	20	8	1

$CaCO_3$ in the laboratory experiments) (15 mL in total, and 5 mL each time). After 1 month, the $CaCO_3$ precipitates were collected from all simulation columns to analyze the mineral components and isotope compositions.

2.5. Mineralogical and microscopic analyses

X-ray diffraction (XRD) was used to analyze the mineral components of the precipitates. After platinum coating in a high-vacuum arc, the crystal morphology of the precipitates was analyzed via scanning electron microscopy-energy dispersive spectroscopy (SEM-EDS). The laboratory samples were analyzed at the Department of Materials and Energy, Southwest University, and the cave in situ samples were analyzed at the Testing Center of the Coalfield Geological Bureau, Sichuan Province.

2.6. Isotopic analysis

The carbon isotope composition of the calcium carbonate precipitates was analyzed with a Thermo Finnigan Delta plus XP mass spectrometer with an online carbonate preparation system (Kiel-IV). The results were reported in per mil (‰) relative to the Vienna Pee Dee Belemnite (VPDB) standard with an analytical precision of typically 0.15‰ for both $\delta^{13}C$ and $\delta^{18}O$ (2σ). The sample analysis was carried out at the Stable Isotope Laboratory of the Institute of Environment and Sustainable Development in Agriculture, Chinese Academy of Agricultural Sciences.

3. Results

3.1. Laboratory experiments

3.1.1. Isolation and identification of strain LHXY2

The 16S rRNA sequence data of strain LHXY2 were uploaded to the NCBI website with accession number MF773945 (Fig. 3). According to the RDP database, most of the isolated bacteria belonged to the genus *Lysinibacillus* (phylum Firmicutes). The phylogenetic tree of LHXY2 and related strains were presented according to the neighbor-joining tree algorithm (MEGA software, Version 6.06) with bootstrap values based on 1000 replications.

3.1.2. The pH value and Ca^{2+} concentration variations and the amount of the precipitates in the laboratory experiments

After 28 d of incubation, accompanied by an increase in the AZ concentration, the pH values and Ca^{2+} concentrations in the laboratory models also showed increasing trends, while the $CaCO_3$ precipitation amounts declined (Fig. 4). The pH values ranged from 8.44 to 8.74, with the highest values occurring in the 1 mmol/L and 8 mmol/L AZ systems. The Ca^{2+} concentrations ranged from 51.9 mmol/L to 104.7 mmol/L, with the highest concentration observed in the 8 mmol/L AZ system. The $CaCO_3$ precipitation amount ranged from 0.02 to

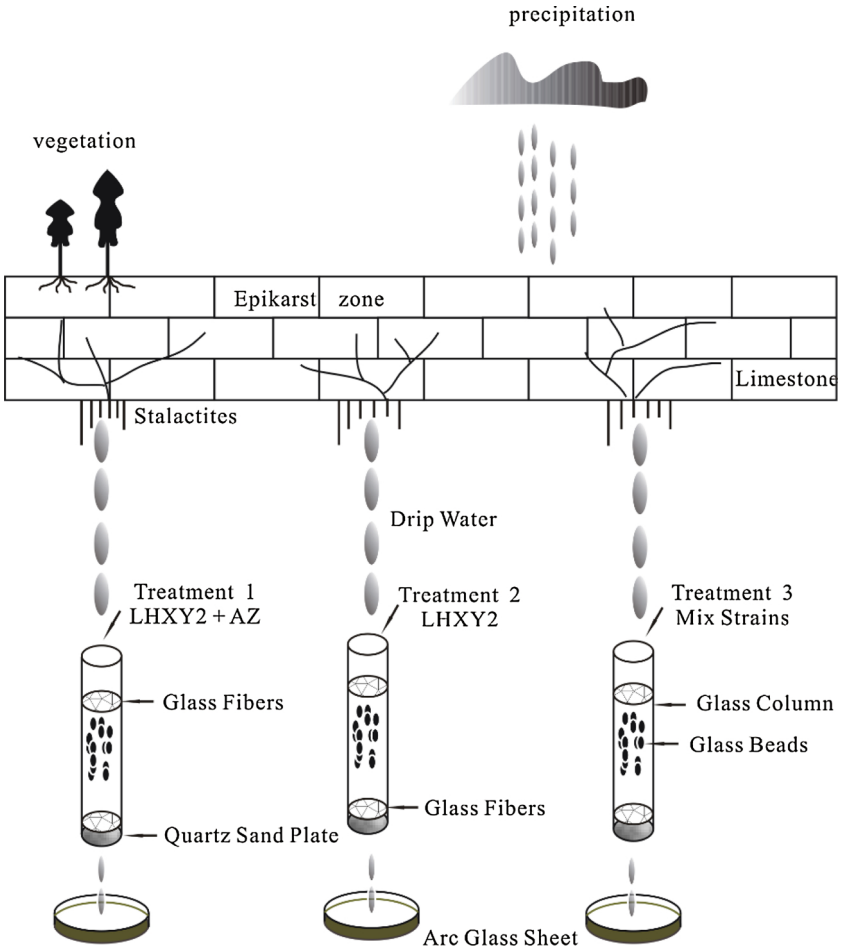

Fig. 2. A simple sketch of the cave in situ experiment for calcium carbonate precipitation in the Xueyu Cave.

0.08, with the maximum weight of 0.08 g occurring in the culture with no AZ addition. The sterilized control revealed an invariable pH value (< 0.1) and Ca^{2+} concentration (< 9.6 mg/L), and the minimum precipitation amount (< 0.005 g).

3.1.3. Mineral components and crystal morphology of the precipitates

Precipitates, which were verified as carbonate minerals, were found in all culture treatments with LHXY2 strain injection but not in those without LHXY2 strain injection, which fully demonstrated that LHXY2 plays an important role in inducing $CaCO_3$ precipitation. The XRD and SEM analysis results indicated that the precipitates collected from the laboratory models were carbonate minerals, including calcite, vaterite and a mixture of calcite and vaterite (Fig. 5). In addition, the mineral components and morphology revealed significant differences in the different AZ concentration treatments, whereby more vaterite and smaller particle diameters were observed in the higher AZ concentration treatments.

Significant mineral crystal morphology differences were observed in the culture media with different AZ concentrations. When there was no AZ (i.e., AZ concentration = 0 mmol/L), the main mineral component was calcite (Fig. 5a), which showed a well-developed rhombohedral crystal structure (Fig. 6a) with a grain size of 5–10 μm. Lian et al. (2006) suggested that microbially induced carbonate minerals exhibited mostly spherical and rhombus forms. When the AZ concentration was 0.5 mmol/L, calcite was also the main mineral component (Fig. 5b), but a small amount of vaterite was observed in the SEM images (Fig. 6b) with a grain size of 10 to 15 μm. When the AZ concentration was 1 mmol/L, calcite also dominated the carbonate components (Fig. 5c), which exhibited radial crystal cross-sections in the SEM images (Fig. 6c), with a crystal grain size between 10–15 μm. When the AZ concentration was 2 mmol/L, vaterite was the main mineral component, while calcite became the minor component (Fig. 5d). The crystals were spherical with a rough surface and a radial cross-

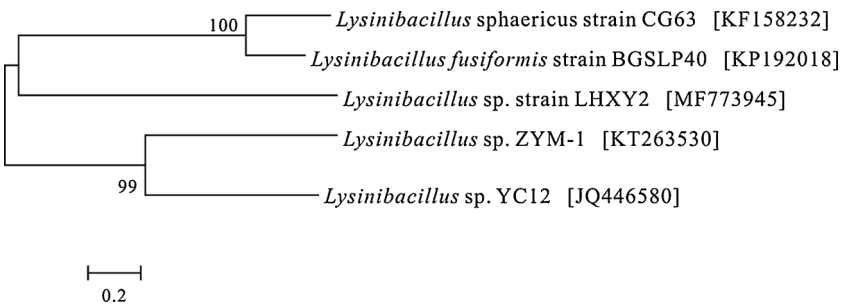

Fig. 3. Phylogenetic tree of *Lysinibacillus* sp. strain LHXY2 based on the 16S rRNA gene sequences according to the neighbor-joining algorithm.

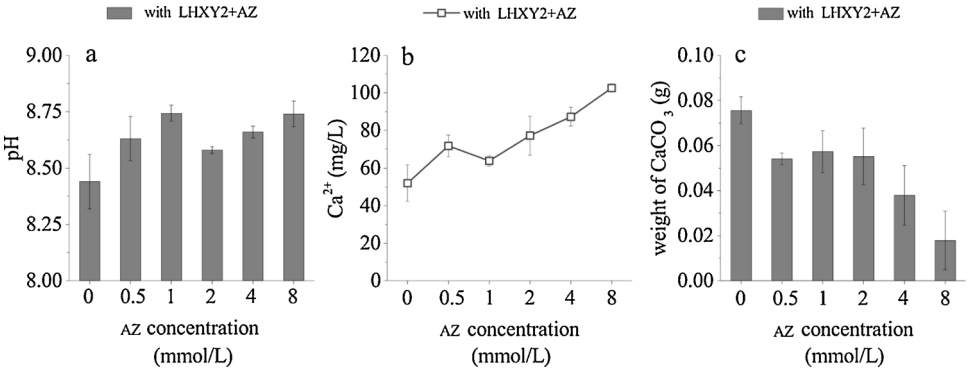

Fig. 4. The pH value, Ca^{2+} concentration and $CaCO_3$ precipitation amount for the different AZ concentrations (all data are the averages of the triplicate experiments).

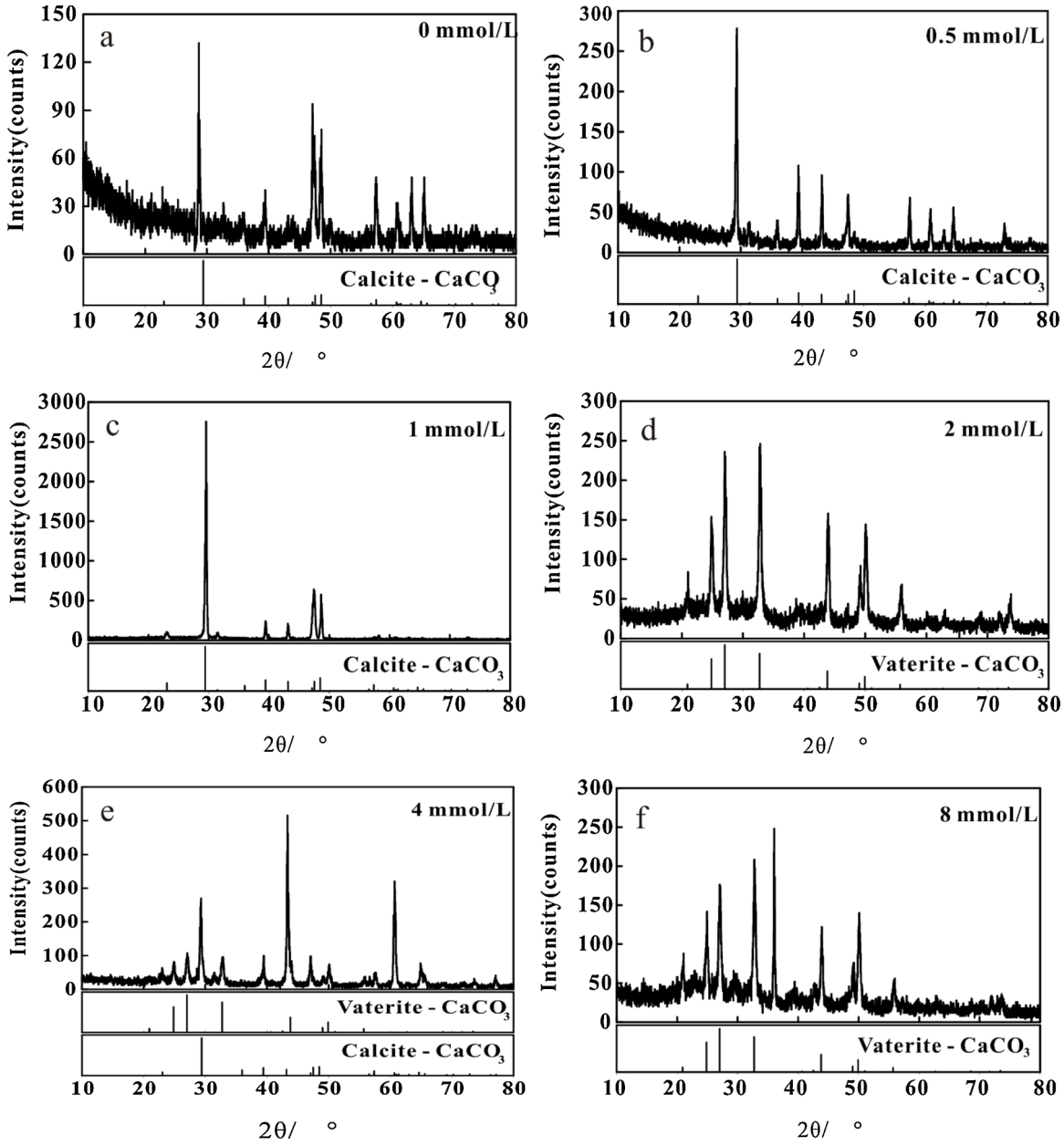

Fig. 5. XRD patterns of the $CaCO_3$ precipitates catalyzed by bacterial CA at the different AZ concentrations.

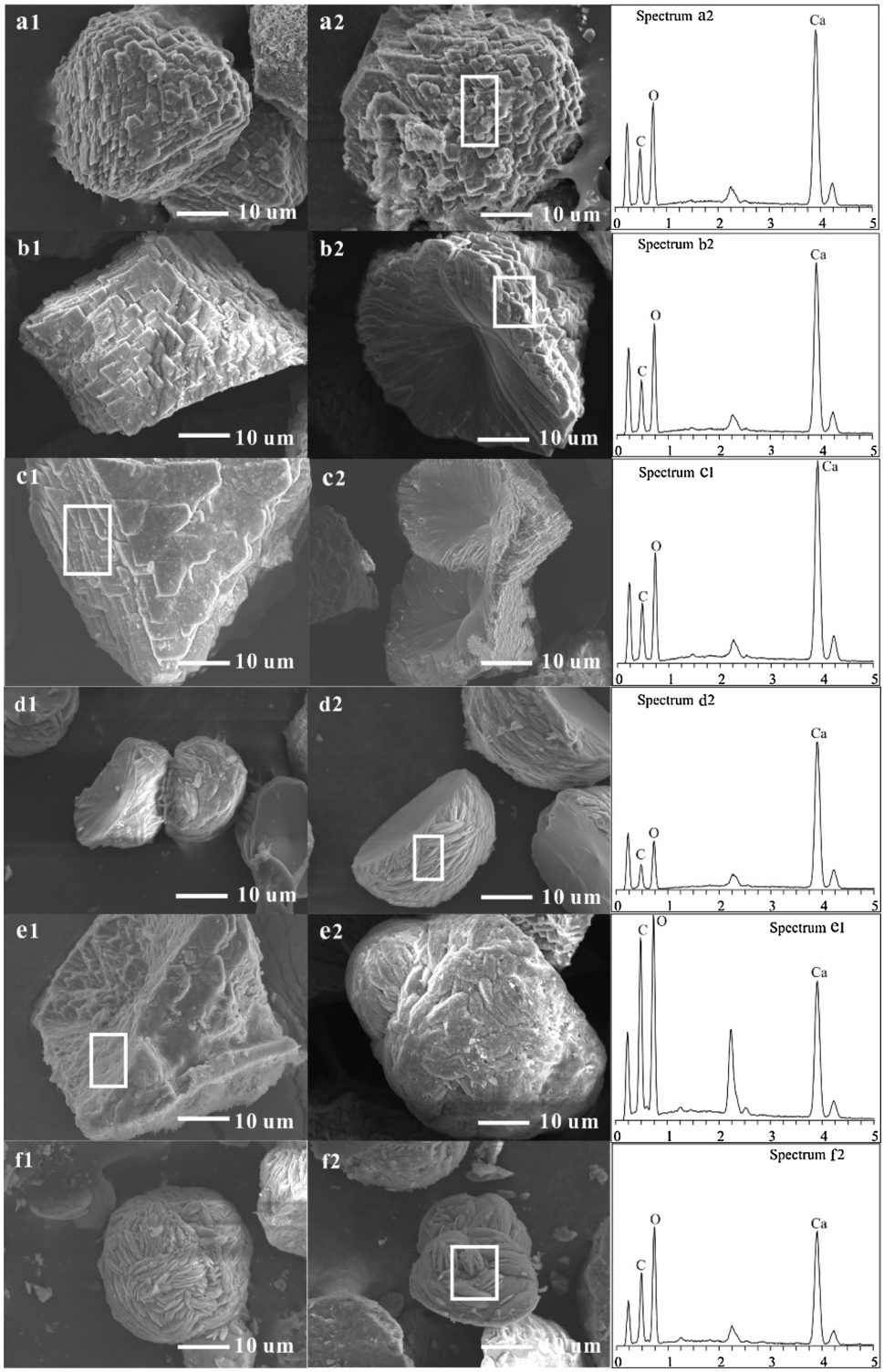

Fig. 6. SEM and EDS images of the $CaCO_3$ precipitates induced by bacterial CA at the different AZ concentrations (the horizontal axis unit is keV, and the vertical axis unit is counts).

section, and the crystal size decreased to 5 ~ 10 μm (Fig. 6d). When the AZ concentration was 4 mmol/L, both calcite and vaterite were formed (Fig. 5e), and tetragonal cones and spherical structures were observed for calcite and vaterite, respectively (Fig. 6e), with a crystal size mostly between approximately 10 and 15 μm. When the AZ concentration was 8 mmol/L, vaterite was the main mineral component (Fig. 5f), and a small amount of calcite was observed in the SEM image (Fig. 6f). The crystal form of the vaterite was spherical with a relatively rough surface, and the size was mostly between approximately 5 and 10 μm.

3.1.4. Carbon isotope composition in the laboratory experiments

The stable isotopes in the carbonate precipitates revealed a significant increasing trend accompanied by an AZ concentration increase in the laboratory models (Fig. 7). The $\delta^{13}C$ values of $CaCO_3$ ranged from −11.79‰ to −4.97‰ with the most positive value of −4.97‰ occurring in the 8 mmol/L AZ treatment, while the $\delta^{18}O$ values of $CaCO_3$ ranged from −10.35‰ to −6.46‰, with the most positive value of -6.46‰ observed in the 8 mmol/L AZ treatment. Compared with the $\delta^{13}C$ value of the $CaCO_3$ in the treatment without AZ, the $\delta^{13}C$ value of

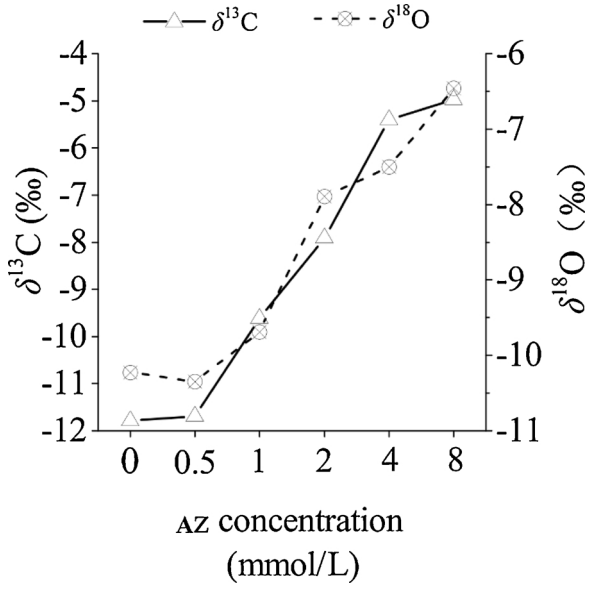

Fig. 7. The $\delta^{13}C$ and $\delta^{18}O$ values of the $CaCO_3$ precipitates induced by the CA produced by strain LHXY2 at the different AZ concentrations.

Table 2
The $\delta^{13}C$ and $\delta^{18}O$ values of the $CaCO_3$ precipitates induced by the CA produced by strain LHXY2 at the different AZ concentrations.

AZ treatments (mmol/L)	$\delta^{13}C$ (‰)	$\delta^{18}O$ (‰)
0	−11.79	−10.23
0.5	−11.69	−10.35
1	−9.62	−9.69
2	−7.91	−7.90
4	−5.40	−7.50
8	−4.97	−6.46

the $CaCO_3$ in the 0.5 mmol/L AZ treatment increased by −0.1‰, that of the $CaCO_3$ in the 2 mmol/L AZ treatment increased by -3.88‰, that of the $CaCO_3$ in the 4 mmol/L AZ treatment increased by −6.39‰ and that of the $CaCO_3$ in the 8 mmol/L AZ treatment increased by -6.82‰. The $\delta^{18}O$ value of $CaCO_3$ also showed the same trend. Compared with the $\delta^{18}O$ value of the $CaCO_3$ in the treatment without AZ, the $\delta^{18}O$ values of the $CaCO_3$ in the 1 mmol/L AZ, 2 mmol/L AZ, 4 mmol/L AZ and 8 mmol/L AZ treatments increased by −0.54‰, −2.33‰, −2.73‰ and −3.77‰, respectively (Table 2). Microbial CA could significantly affect isotope fractionation in the microbial-induced $CaCO_3$ precipitation process. The stable carbon isotope analysis showed that the CA produced by the *Lysinibacillus* sp. strain LHXY2 resulted in an approximately −7‰ $\delta^{13}C$ variability. The $\delta^{18}O$ value trend was consistent with that of the $\delta^{13}C$ values, with an approximately −4‰ $\delta^{18}O$ variability.

3.2. Cave in situ experiments

3.2.1. Mineral components

According to the d values of the semiquantitative XRD analysis, the $CaCO_3$ precipitates collected after 30 d from the in situ cultures consisted of calcite. The d value of $CaCO_3$ precipitation was 3.03 nm (Fig. 8) in the three cave in situ experiments, which coincided with the d value of calcite ($CaCO_3$, 3.03 nm). The maximum $CaCO_3$ precipitation amount was 0.49 g collected from treatment 3, followed by the 0.41 g collected from treatment 2, and the minimum precipitation amount of 0.26 g was collected from treatment 1 (Table 3).

3.2.2. Stable isotope composition

The cave in situ experiments showed that the carbon isotope composition of the $CaCO_3$ precipitates induced by *Lysinibacillus* sp. LHXY2 was significantly dependent on the AZ concentration. In treatment 1 with the addition of AZ, *Lysinibacillus* sp. LHXY2 CA production was inhibited; therefore, the $\delta^{13}C$ value was −10.34‰, and the $\delta^{18}O$ value was −5.81‰. In treatment 2 with *Lysinibacillus* sp. LHXY2 CA production, the $\delta^{13}C$ and $\delta^{18}O$ values were -11.74 ‰ and -6.03 ‰, respectively. In treatment 3 with the mixed strains (XYQE, XY31, and XYLG), the $\delta^{13}C$ and $\delta^{18}O$ values were −10.81 ‰ and −5.79 ‰, respectively (Table 3).

4. Discussion

4.1. Comparative analysis of the laboratory and cave in situ experiments

4.1.1. Hydrochemical analysis in the laboratory experiment

CA catalyzed the reversible reaction of $CO_2+H_2O \leftrightarrow H^+ + HCO_3^-$, which played an important role in $CaCO_3$ precipitation. When the activity of CA was inhibited, the $CaCO_3$ precipitation process was also inhibited, which was observed from the variations in the pH value, soluble Ca^{2+} concentration and $CaCO_3$ precipitation amount (Fig. 4). Microbial CA might be the dominant driving factor of the pH value variations. The pH value before incubation was 8.0 as determined by calcium acetate and yeast paste. Calcium acetate can be a weakly acidic or strongly alkali salt, whereas the yeast paste, the main component of the organic nitrogen source, might lead to an alkaline solution after hydrolysis (Guo et al., 2013). The pH value increase could be due to CA and other complex microbial physical and chemical reactions (Xie and Wu, 2014). As shown in Fig. 4, the pH value increased significantly in the laboratory model with injection of strain LHXY2 (by 1.38 units compared to the blank), which might be related to the activity of CA and other microbial reactions. Moreover, the addition of inhibitor AZ contributed to the CA activity decline, and the hydration reaction ($CO_2+H_2O \leftrightarrow H^+ + HCO_3^-$) slowed down or was stopped; thus, the H^+ concentration decreased and the pH value increased even more significantly.

The decline in Ca^{2+} concentration coincided with the increase in the $CaCO_3$ precipitation amount and revealed an opposite trend with the AZ addition amount, which indicated that CA was the most notable carbonate mineralization driving factor, not the pH. A marked increase in the Ca^{2+} concentration was observed in the 8 mmol/L AZ treatment, accompanied by the minimum $CaCO_3$ precipitation amount and highest pH value. In contrast, the maximum $CaCO_3$ precipitation amount was collected from the treatment without AZ addition, in which the pH value remained low and the Ca^{2+} concentration decreased the most. Although a higher pH value promoted carbonate mineral formation, the highest pH value observed in the highest AZ addition treatment did not result in a large $CaCO_3$ precipitation amount, which indicated that the pH was not the main factor under CA inhibition conditions. Because of the AZ addition, the mutual conversion reaction between CO_2 and HCO_3^- was slowed down, the insufficient carbonate level influenced the mineralization induced by microorganisms (Wang et al., 2010), and consequently, the $CaCO_3$ precipitation amount was reduced (Moulin et al., 2011).

The correlations between the AZ concentration and the pH value, Ca^{2+} concentration and $CaCO_3$ precipitation amount also revealed the control of the AZ concentration on carbonate mineral precipitation (Fig. 9). The AZ concentration was positively correlated with the pH value and Ca^{2+} concentration of the cell culture medium (r = 0.55 and 0.87, respectively) but negatively correlated with the $CaCO_3$ precipitation amount (r = -0.81), which indicated that AZ significantly affected carbonate precipitation and that the pH value showed little effect on carbonate precipitation after the addition of the inhibitor AZ. The pH value might be influenced by four possible mechanisms: (1) bacterial metabolism and secretion of low-molecular-weight organic acids; (2) CO_2 dissolved in water and subsequently participated in a series of $CaCO_3$ precipitation reactions: $CO_2+H_2O \rightarrow H_2CO_3$; $H_2CO_3 \rightarrow HCO_3^- + H^+$; $HCO_3^- \rightarrow CO_3^{2-} + H^+$; $CO_3^{2-} + Ca^{2+} \rightarrow CaCO_3$; (3) autolysis of dead bacteria; and (4) bacterial consumption of organic nitrogen sources and ammonia production, which dissolves in water and releases OH^- (Guo

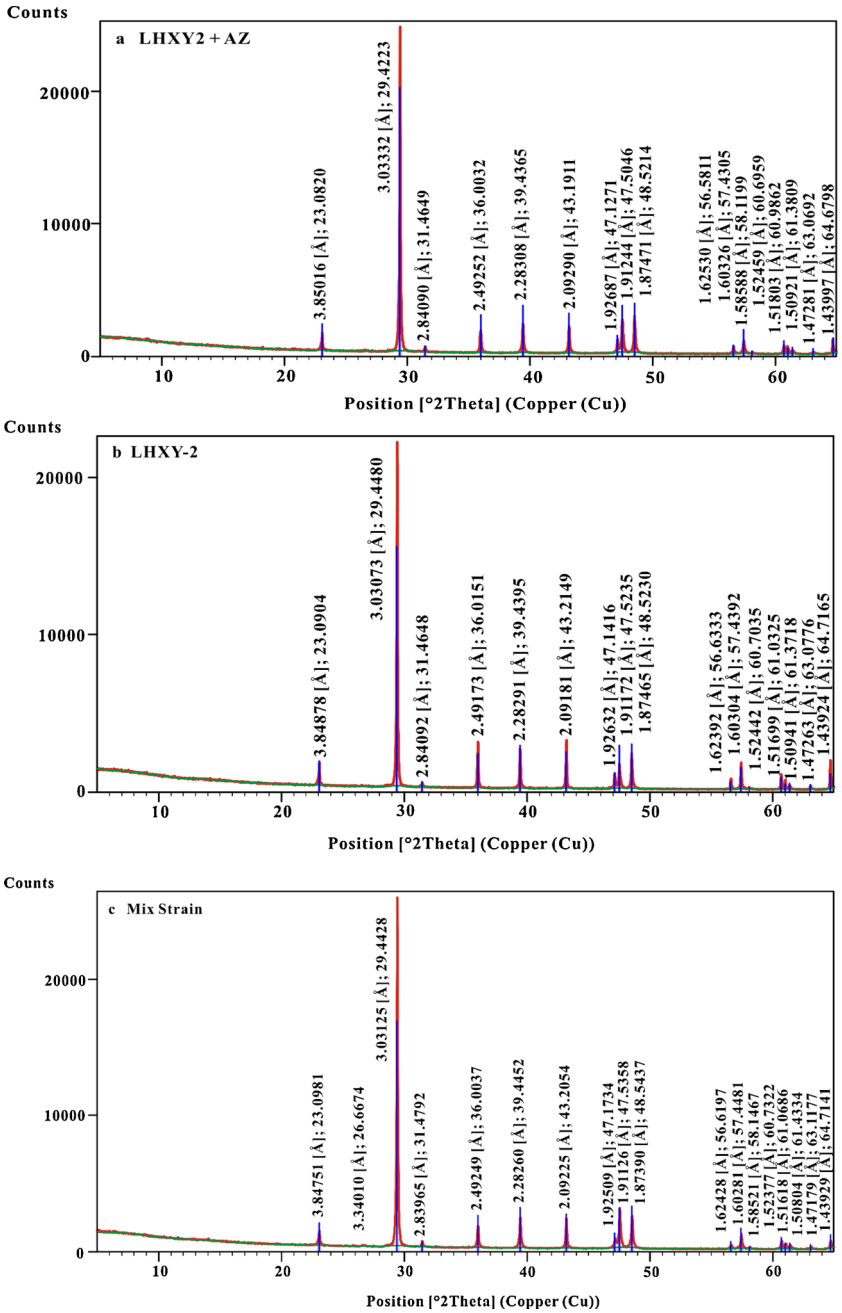

Fig. 8. Mineral components of the $CaCO_3$ precipitates from the cave in situ experiments.
In the figure, a, b and c refer to treatments 1, 2 and 3, respectively. The red line is the peak strength of the sample, the blue line is the standard peak, and the green line is the baseline. The value of 3.03 nm (Fig. 8a) refers to the d value of the semiquantitative XRD analysis. (For interpretation of the references to colour in this figure legend, the reader is referred to the web version of this article.)

Table 3
The amount and $\delta^{13}C$ and $\delta^{18}O$ values of the $CaCO_3$ precipitates in the cave in situ experiments.

Treatments	$CaCO_3$ precipitation amount (g)	$\delta^{13}C$ (‰)	$\delta^{18}O$ (‰)
LHXY2 + AZ	0.26	−10.34	−5.81
LHXY2	0.41	−11.74	−6.03
Mixed strains	0.49	−10.81	−5.79

et al., 2013). According to the second mechanism mentioned above, the CO_2 sources might include the CO_2 derived from bacterial respiration and CO_2 from air. Our experiment prevented CO_2 sourcing from air; therefore, the CO_2 involved in the hydration reaction is mainly derived from bacterial respiration (Xu et al., 2017). CA promoted the combination of CO_2 and H_2O into H_2CO_3 and further decomposed the H_2CO_3 into HCO_3^- and H^+. In the treatment without AZ, the accumulation of HCO_3^- and H^+ provided H^+ for microbial redox reactions and further decomposed HCO_3^- into CO_3^{2-} for $CaCO_3$ precipitation. In the high-AZ treatment, HCO_3^- decomposition declined due to CA catalysis and was inhibited; thus, the insufficient CO_3^{2-} led to a decrease in $CaCO_3$ precipitation, and the precipitation amount decreased accordingly.

4.1.2. Differences in the mineral components of the $CaCO_3$ precipitates

Calcite is thermodynamically stable, while vaterite is the metastable phase of $CaCO_3$ (Zhou et al., 2010a). Carbonate mineral precipitation varied in the different AZ treatments, which indicated that the $CaCO_3$

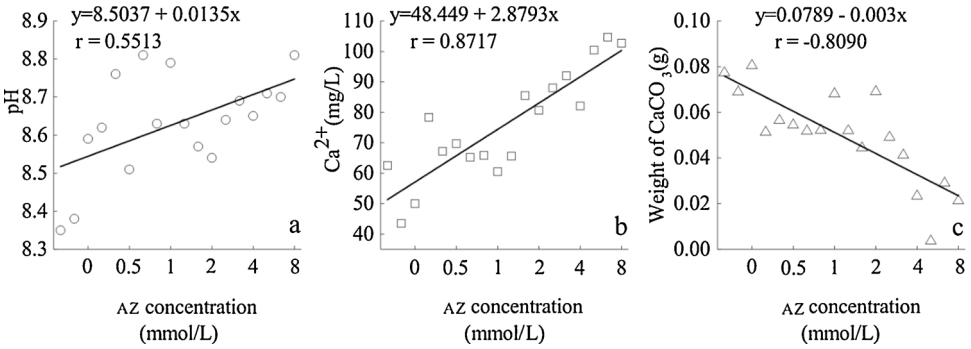

Fig. 9. Correlations between the AZ concentration and the pH value, calcium concentration, and $CaCO_3$ precipitation amount.

morphology in the laboratory model might be related to the mineralization sites of bacteria and that CA affected the hydrocarbonate concentrations. Lian et al. (2008) found that the environmental conditions of bacteria, metabolites and their surrounding nutrients significantly affected the crystal morphology of calcite. Zhou et al. (2010b) showed that large-particle calcite was formed with a smooth surface when bacteria were cultured without nitrogen in the calcite crystallization system, whereas small-particle calcite was formed with a rough surface when bacteria were cultured with nitrogen. Li et al. (2011a) showed that *Bacillus mucilaginosus* led to $CaCO_3$ precipitation while apatite was decomposed as the only source of calcium and phosphorus, which was associated with the strong cation adsorption capacity of bacteria and the ability to produce CA and promote CO_2 hydration (Chen and Lian, 2005; Lian et al., 2008).

The mineral components of the modern speleothems in the Xueyu Cave are primarily composed of calcite with trigonal lattice crystal particles, most of which are aggregates of relict crystals and occasional single complete crystals on the precipitate dispersion edge. There was no notable difference in the calcite crystals formed in different seasons (Wu et al., 2015). Our results showed that differences had been observed in the mineral components and crystal forms between the different AZ concentration treatments with LHXY2 strain injection. The mineral components were mainly composed of calcite, vaterite or a mixture of calcite and vaterite. The calcium carbonate consisted of petal-shaped and funnel-shaped crystals, which differed from the trigonal lattice particles formed at the cave drip water sites. Since the crystal morphology was influenced not only by the surrounding environment but also by many other factors, such as the microbial exudates, the pH of the culture medium and the ions added, the bacteria induced a variety of different crystal forms in the laboratory experiment. Wang et al. (2010) reported that microorganisms had an escape mechanism in the process of calcium carbonate mineralization, which might ultimately influence the precipitation of carbonate minerals. In addition, traces of microbial activities on the surfaces of crystals were clearly observed, which further indicated that microbial activities had an important effect on $CaCO_3$ precipitation.

4.1.3. Differences in the carbon isotope composition of the $CaCO_3$ precipitates

Microbial CA could significantly influence stable isotope fractionation in modern speleothems. The $\delta^{13}C$ and $\delta^{18}O$ values of the $CaCO_3$ in the laboratory models and cave in situ simulations demonstrated the influence of the microbial CA. According to the laboratory models, the approximately −7‰ $\delta^{13}C$ and −4‰ $\delta^{18}O$ deviations were attributed to CA (Fig. 7), as the $\delta^{13}C$ and $\delta^{18}O$ values revealed a significant increase under the condition that the CA activity was inhibited by the high concentration of AZ. We propose that CA had the ability to promote hydrocarbonate conversion and accelerated $CaCO_3$ precipitation; thus, the stable isotopes in $CaCO_3$ might exhibit less deviation because of the rapid precipitation process and decreased fractionation.

Compared with the modern speleothems in the Xueyu Cave, the $CaCO_3$ collected from the cave in situ experiments revealed relatively positive $\delta^{13}C$ and $\delta^{18}O$ values, and the $\delta^{13}C$ and $\delta^{18}O$ values of the $CaCO_3$ collected from the AZ system were even more positive than those of the $CaCO_3$ collected from the system without AZ. The $\delta^{13}C$ values of the modern speleothems ranged from −13.80‰ to −12.96‰, with an average of −13.18‰ at the microorganism sampling sites in the cave (Table 4). The $\delta^{18}O$ values of the modern speleothems ranged from -6.90‰ to -6.13‰, with an average of -6.6‰ at the microorganism sampling sites. The $\delta^{13}C$ value of treatment 2 (LHXY2 injection without AZ) among the cave in situ experiments is -11.74‰ (Table 3), which is -2‰ more positive than that of modern speleothems, while the $\delta^{18}O$ value of treatment 2 is -6.03‰ and -0.6‰ more positive than those of modern speleothems. The reason might be that in the cave in situ experiments, the drip water process was dynamic, and thus, the interaction between the bacteria and drip water had a greater influence on the CAex activity of the bacteria in the open cave environment. The elevation in $\delta^{13}C$ and $\delta^{18}O$ values of treatment 2 indicated microbial mineralization fractionation during $CaCO_3$ precipitation. However, the even more positive $\delta^{13}C$ and $\delta^{18}O$ values of treatment 1 (LHXY2 injection with AZ) revealed a similar phenomenon to that in the laboratory model, which was that the $\delta^{13}C$ and $\delta^{18}O$ values were −1.4‰ and −0.2‰, respectively, more positive than those of treatment 2, and the $CaCO_3$ precipitation amount was smaller than that in treatment 2. The variations in the AZ treatments indicated CA-induced precipitation acceleration and negative isotope fractionation. Such isotope fractionation could cause a large uncertainty in the reconstruction of paleoenvironmental changes based on speleothem isotope compositions.

4.2. Effect of microbial mediation on calcium carbonate precipitation

According to the literature, microbial actions were involved in moonmilk and calcite precipitation, which led to stable isotope fractionation. Maciejewska et al. (2017) reported that filamentous *Streptomyces* could act as nucleation sites in moonmilk formation. In addition, the metabolic activities involved in $CaCO_3$ precipitation were evaluated by in vitro cultures of moonmilk *Streptomyces*. It was found

Table 4
The $\delta^{13}C$ and $\delta^{18}O$ values of the speleothem precipitates at the microorganism sampling sites.

D1	$CaCO_3$ precipitation amount (g)	$\delta^{13}C$ (‰)	$\delta^{18}O$ (‰)
2015.05-2015.07	0.15	−13.23	−6.22
2015.07-2015.09	0.29	−12.96	−6.13
2015.09-2015.11	0.31	−13.39	−6.63
2015.11-2015.12	0.03	−13.22	−6.78
2015.12-2016.02	1.76	−13.00	−6.78
2016.02-2016.03	0.65	−13.08	−6.90
2016.03-2016.04	0.12	−13.23	−6.75
2016.04-2016.05	0.21	−13.20	−6.77
2016.05-2016.07	0.23	−13.34	−6.43
mean	/	−13.80	−6.60
sum	3.76	/	/

Table 5
The $\delta^{13}C$ values of the vegetation and soil CO_2 above the Xueyu Cave and the *DIC* of the drip water in the cave.

Sample	$\delta^{13}C$ (‰)	n
vegetation	−30.99	n = 3
soil	−23.37	n = 3
soil CO_2	−19.08	n = 3
atmospheric CO_2	−9.00	n = 3
cave-air CO_2	−20.00	n = 2
Drip site D1	−10.47	n = 7
Drip site D4	−12.07	n = 9

Table 6
Comparison of the speleothem precipitation amounts in the Xueyu Cave (unit: g).

Time	Drip water	$CaCO_3$ precipitation amount (g)	$\delta^{13}C$ (‰) mean	$\delta^{18}O$ (‰) mean
2015.05-2015.11	D1	0.75	−13.19	−6.33
	D4	0.25	−10.95	−7.09
2015.11-2016.05	D1	2.78	−13.15	−6.80
	D4	0.96	−10.64	−6.86

that peptide/amino acid ammonification and a small amount of ureolysis could the preferential metabolic pathways participating in carbonate precipitation by increasing the pH of the bacterial environment. The stable isotope composition of the moonmilk precipitate ($\delta^{18}O$ value: −4.9‰ to −9.1‰; $\delta^{13}C$ value: −9.5‰ to −14.5‰) indicated significant incorporation of the organically derived CO_2 and probably a biological influence on the calcite crystals (Sanchez-Moral et al., 2012). Zhuang et al. (2018) studied the biotic calcite precipitation induced by the microorganism *Bacillus cereus* MRR2, and more negative $\delta^{13}C$ values (-20.9 ‰) were found than those of organogenic calcite (-15.6‰) and inorganogenic calcite (-11.7‰), suggesting that microbial activities strongly affected the carbon isotope composition of biotic calcite. Our research demonstrated a similar influence of microbial fractionation.

In general, the $\delta^{13}C$ values of speleothems were determined by the $\delta^{13}C$ values of the dissolved inorganic carbon (*DIC*) produced by the dissolution of Cretaceous marine limestones and dolostones (host rock) by the carbonic acid derived from the soil CO_2 and atmospheric CO_2. Commonly, the $\delta^{13}C$ value of the overlying deciduous vegetation was −30.99‰ (n = 3), of which the CO_2 from soil organic material respiration was −23.37‰ on average (n = 3). The $\delta^{13}C_{CO2}$ value of CO_2 in the overlying soil was −19.08‰ (n = 3). The $\delta^{13}C$ value of the atmospheric CO_2 was close to -9‰ (n = 3), whereas the $\delta^{13}C$ value of the cave-air CO_2 in the Xueyu Cave was −20.00‰ (n = 2) (Table 5). From July 2015 to June 2016, the $\delta^{13}C_{DIC}$ values of the drip water (Table 5) ranged from −10.25‰ to −15.18‰, with an average of −11.47‰ at drip site D1, and ranged from −10.01‰ to −14.68‰, with an average of −12.07‰ at drip site D4. The $\delta^{13}C_{DIC}$ value was mainly affected by changes in the soil CO_2 and the $\delta^{13}C$ values of the bedrock. The amount of drip water was mainly affected by rainfall, and in the rainy season, rainfall infiltrates rapidly and carries more isotope-depleted soil CO_2 with the drip water. In the dry season, the $\delta^{13}C_{CO2}$ value of the soil had increased, as had the $\delta^{13}C_{DIC}$ value of the drip water. The $\delta^{13}C$ values of the modern speleothems ranged from −10.65‰ to −13.39‰ with an average of −12.93‰ at drip site D1 and ranged from −10.38‰ to −11.07‰ with an average of −10.79‰ at drip site D4 (Table 6).

We used the Dienes equation (Dienes et al., 1974; Mickler et al., 2004) to calculate the fractionation temperature. The equation is presented as follows:

$$1000 \ln \alpha_{calcite\text{-}HCO3^-} = 0.095(10^6 * T^2) + 0.90 \quad (1)$$

$$\alpha_{calcite\text{-}HCO3^-} = (\delta_{calcite} + 1000) / (\delta_{HCO3^-} + 1000) \quad (2)$$

where $\alpha_{calcite\text{-}HCO3^-}$ refers to the fractionation coefficient between calcite and medium water, namely, $(\delta_{calcite} + 1000) / (\delta_{HCO3^-} + 1000)$, $\delta_{calcite}$ denotes the $\delta^{13}C$ value of calcium carbonate, δ_{HCO3^-} is the $\delta^{13}C$ value of the medium water, and T is the temperature in Kelvin.

In our study, the pH values of the drip water ranged from 7.2 to 8.1 at drip site D1 and from 7.4 to 8.1 at drip site D4 from July 2015 to June 2016, so the *DIC* of the drip water in the Xueyu Cave was primarily composed of HCO_3-. The carbon isotope fractionation equilibrium was calculated using the $\delta^{13}C_{DIC}$ values of the drip water at drip sites D1 and D4 and the $\delta^{13}C$ values of the modern speleothems from July 2015 to June 2016. The equilibrium fractionation coefficients are shown in Table 7.

The theoretical carbon isotope fractionation equilibrium of the Xueyu Cave was inversely determined using the Dienes equation.

5. Conclusions

Lysinibacillus sp. strain LHXY2 was used in the laboratory and cave in situ simulation experiments to demonstrate the microbial CA influence on calcium carbonate precipitation and microbially induced stable isotope fractionation. The results showed that the microbial CA influenced the precipitation amount, crystal morphology and $\delta^{13}C$ and $\delta^{18}O$ values in speleothem precipitation. *Lysinibacillus* sp. strain LHXY2 produced CAex, contributed substantially to calcium carbonate precipitation, and influenced the $\delta^{13}C$ and $\delta^{18}O$ values in the laboratory and cave in situ simulation experiments. The CA activity of strain LHXY2 resulted in approximately -7‰ $\delta^{13}C$ and -4‰ $\delta^{18}O$ variabilities in the laboratory experiments and led to an approximately -1.4‰ $\delta^{13}C$ shift in the cave in situ experiments. Our results highlight the importance of microbially induced fractionation, which can lead to significant negative $\delta^{13}C$ deviations. Therefore, microbial activities should be considered when using the speleothem carbon isotope composition to reconstruct the paleoenvironment.

Declaration of Competing Interest

The authors declare that they have no known competing financial interests or personal relationships that could have appeared to influence the work reported in this paper.

The authors declare the following financial interests/personal relationships which may be considered as potential competing interests.

Acknowledgments

This study was financially supported by the National Key Research and Developmental Program of China (2016YFC0502306) and the Chongqing Municipal Science and Technology Commission Fellowship Fund (CSTC2018jcyj-yszx0013, CSTC2017jcyj-ysxx0004). Thanks are given to Prof. Daoxian Yuan, Prof. Tingyong Li and Dr. Xinyi Xiang from the School of Geographical Sciences, Southwest University, Prof. Yongqin Liu, Prof. Juzhi Hou, Dr. Mukan Ji and Dr. Liang Shen from the Institute of Tibetan Plateau Research, Chinese Academy of Sciences, Dr. Kunyu Wu from the Research Institute of Petroleum Exploration and Development, Qinghai Oil

Table 7
Determination of carbon isotope fractionation in the Xueyu Cave.

drip water	T_{mean} (K)	calculation value $\alpha_{calcite\text{-}HCO3^-}$	$\delta^{13}C_{calcite}$ (‰) mean	$\delta^{13}C_{HCO3^-}$ (‰) mean	$(\delta_{calcite} + 1000) / (\delta_{HCO3^-} + 1000)$
D1	292.6	1.00	−12.64	−10.74	0.99
D4	292.7	1.00	−10.78	−11.27	1.00

Field, CNPC, I gratefully acknowledge their guidance and help. Thanks are also given to Jiaqi Lei, Liuchan Hu, Sibo Zeng and Ze Zeng from the School of Geographical Sciences, Southwest University, who contributed with the fieldwork. We thank two anonymous reviewers for their thoughtful and detailed comments, which helped to improve the manuscript. Finally, we highly appreciate the editorial work.

References

Boquet, E., Boronat, A., Ramos-Cormenzana, A., 1973. Production of calcite (calcium carbonate) crystals by soil bacteria is a general phenomenon. Nature 246 (5434), 527.

Chen, Y., Lian, B., 2005. Ability of *Bacillus mucilaginosus* GY03 strain to adsorb chromium ions. Pedosphere 15 (2), 225–231.

Cheng, H., et al., 2016. The Asian monsoon over the past 640,000 years and ice age terminations. Nature 534 (7609), 640–646.

Dhami, N.K., Mukherjee, A., Watkin, E.L., 2018. Microbial diversity and mineralogical-mechanical properties of calcitic cave speleothems in natural and in vitro biomineralization conditions. Front. Microbiol. 9, 40.

Dienes, P., Langmuir, D., Harmon, R., 1974. Stable carbon isotope ratios and existence of a gas phase in the evolution of carbonate groundwater. Geochim. et Comochim. Acta 38, 1147–1164.

Dredge, J., et al., 2013. Cave aerosols: distribution and contribution to speleothem geochemistry. Quat. Sci. Rev. 63, 23–41.

Engel, A.S., et al., 2010. Linking phylogenetic and functional diversity to nutrient spiraling in microbial mats from Lower Kane Cave (USA). ISME J. 4 (1), 98–110.

Fohlmeister, J., et al., 2018. Carbon and oxygen isotope fractionation in the water-calcite-aragonite system. Geochim. et Cosmochim. Acta.

Guo, W., et al., 2013. *Citrobacter* sp. strain GW-M mediates the coexistence of carbonate minerals with various morphologies. Geomicrobiol. J. 30 (8), 749–757.

Hansen, M., Scholz, D., Froeschmann, M.-L., Schöne, B.R., Spötl, C., 2017. Carbon isotope exchange between gaseous CO_2 and thin solution films: artificial cave experiments and a complete diffusion-reaction model. Geochim. et Cosmochim. Acta 211, 28–47.

Jimenez-Lopez, C., Rodriguez-Navarro, A., Dominguez-Vera, J.M., Garcia-Ruiz, J.M., 2003. Influence of lysozyme on the precipitation of calcium carbonate: a kinetic and morphologic study. Geochim. et Cosmochim. Acta 67 (9), 1667–1676.

Kanth, B.K., et al., 2012. Expression and characterization of codon-optimized carbonic anhydrase from *Dunaliella* species for CO_2 sequestration application. Appl. Biochem. Biotechnol. 167 (8), 2341–2356.

Kele, S., et al., 2015. Temperature dependence of oxygen-and clumped isotope fractionation in carbonates: a study of travertines and tufas in the 6–95°C temperature range. Geochim. et Cosmochim. Acta 168, 172–192.

Kim, I.G., et al., 2012. Biomineralization-based conversion of carbon dioxide to calcium carbonate using recombinant carbonic anhydrase. Chemosphere 87 (10), 1091–1096.

Kimble, J.C., Winter, A.S., Spilde, M.N., Sinsabaugh, R.L., Northup, D.E., 2018. A potential central role of *Thaumarchaeota* in N-Cycling in a semi-arid environment, Fort Stanton Cave, Snowy River passage, New Mexico, USA. FEMS Microbiol. Ecol. 94 (11), fiy173.

Kondratyeva, L., Polevskaya, O., Litvinenko, Z., Golubeva, E., Konovalova, N., 2016. Role of the microbial community in formation of speleothem (moonmilk) in the Snezhnaya carst cave (abkhazia). Microbiology 85 (5), 629–637.

Li, H., et al., 1997. Interannual-resolution $\delta^{13}C$ record of stalagmites as proxy for the changes in precipitation and atmospheric CO_2 in Shihua Cave, Beijing. Carsologica Sinica 16 (4), 285–295 (in Chinese).

Li, H., Lian, B., Gong, G., Du, K., 2011a. The formation of calcium carbonate particles induced by bacteria. Geol. J. China Univ. 17 (01), 112–117 (in Chinese).

Li, T., et al., 2011b. Transportation characteristics of $\delta^{13}C$ in the plants-soil-bedrock-cave system in Chongqing karst area. Sci. China Earth Sci. 55 (4), 685–694.

Lian, B., et al., 2008. Microbial flocculation by *Bacillus mucilaginosus*: applications and mechanisms. Bioresour. Technol. 99 (11), 4825–4831.

Lian, B., Hu, Q., Chen, J., Ji, J., Teng, H.H., 2006. Carbonate biomineralization induced by soil bacterium *Bacillus megaterium*. Geochim. et Cosmochim. Acta 70 (22), 5522–5535.

López-Moreno, A., Sepúlveda-Sánchez, J.D., Alonso, Mercedes, Guzmán, E.M., Le Borgne, S., 2014. Calcium carbonate precipitation by heterotrophic bacteria isolated from biofilms formed on deteriorated ignimbrite stones: influence of calcium on EPS production and biofilm formation by these isolates. Biofouling 30 (5), 547–560.

Maciejewska, M., et al., 2017. Assessment of the potential role of *Streptomyces* in cave moonmilk formation. Front. Microbiol. 8, 1181.

Mickler, P.J., et al., 2004. Stable isotope variations in modern tropical speleothems: Evaluating equilibrium vs. kinetic isotope effects. Geochim. et Cosmochim. Acta 68 (21), 4381–4393.

Millo, C., et al., 2012a. Carbon isotope fractionation during calcium carbonate precipitation induced by urease-catalysed hydrolysis of urea. Chem. Geol. 330, 39–50.

Millo, C., et al., 2012b. Carbon isotope fractionation during calcium carbonate precipitation induced by ureolytic bacteria. Geochim. et Cosmochim. Acta 98, 107–124.

Moulin, P., Andría, J.R., Axelsson, L., Mercado, J.M., 2011. Different mechanisms of inorganic carbon acquisition in red macroalgae (Rhodophyta) revealed by the use of TRIS buffer. Aquat. Bot. 95 (1), 31–38.

Okyay, T.O., Rodrigues, D.F., 2015. Biotic and abiotic effects on CO_2 sequestration during microbially-induced calcium carbonate precipitation. FEMS Microbiol. Ecol. 91 (3).

Ortiz, M., et al., 2014. Making a living while starving in the dark: metagenomic insights into the energy dynamics of a carbonate cave. ISME J. 8 (2), 478.

Portillo, M.C., Gonzalez, J.M., 2011. Moonmilk deposits originate from specific bacterial communities in Altamira Cave (Spain). Microbial Ecol. 61 (1), 182–189.

Power, I.M., Harrison, A.L., Dipple, G.M., 2016. Accelerating mineral carbonation using carbonic anhydrase. Environ. Sci. Technol. 50 (5), 2610–2618.

Power, I.M., Harrison, A.L., Dipple, G.M., Southam, G., 2013. Carbon sequestration via carbonic anhydrase facilitated magnesium carbonate precipitation. Int. J. Greenhouse Gas Control 16, 145–155.

Riding, R., 2006. Cyanobacterial calcification, carbon dioxide concentrating mechanisms, and Proterozoic-Cambrian changes in atmospheric composition. Geobiology 4 (4), 299–316.

Rusznyak, A., et al., 2011. Calcite biomineralization by bacterial isolates from the recently discovered pristine karstic herrenberg cave. Appl. Environ. Microbiol. 78 (4), 1157–1167.

Sanchez-Moral, S., et al., 2012. The role of microorganisms in the formation of calcitic moonmilk deposits and speleothems in Altamira Cave. Geomorphology 139, 285–292.

Sánchez-Román, M., Puente-Sánchez, F., Parro, V., 2015. Nucleation of Fe-rich phosphates and carbonates on microbial cells and exopolymeric substances. Front. Microbiol. 6, 1024.

Smith, K.S., Ferry, J.G., 2000. Prokaryotic carbonic anhydrases. FEMS Microbiol. Rev. 24 (4), 335–366.

Swarnalatha, G., Hegde, N.S., Chauhan, V.S., Sarada, R., 2015. The effect of carbon dioxide rich environment on carbonic anhydrase activity, growth and metabolite production in indigenous freshwater microalgae. Algal Res.-Biomass Biofuels Bioprod. 9, 151–159.

Tebo, B.M., et al., 2015. Microbial communities in dark oligotrophic volcanic ice cave ecosystems of Mt. Erebus, Antarctica. Front. Microbiol. 6, 179.

Tran, M.-K., et al., 2013. Lysozyme encapsulation within PLGA and $CaCO_3$ microparticles using supercritical CO_2 medium. J. Supercrit. Fluids 79, 159–169.

Uchikawa, J., Zeebe, R.E., 2012. The effect of carbonic anhydrase on the kinetics and equilibrium of the oxygen isotope exchange in the CO_2-H_2O system: implications for $\delta^{18}O$ vital effects in biogenic carbonates. Geochim. et Cosmochim. Acta 95, 15–34.

Versteegh, E., Black, S., Hodson, M.E., 2017. Carbon isotope fractionation between amorphous calcium carbonate and calcite in earthworm-produced calcium carbonate. Appl. Geochem. 78, 351–356.

Wang, H., et al., 2010. Calcium carbonate precipitation induced by a bacterium strain isolated from an oligotrophic cave in Central China. Front. Earth Sci. 4 (2), 148–151.

Wang, Y., et al., 2001. A high-resolution absolute-dated Late Pleistocene monsoon record from Hulu Cave, China. Science 294 (5550), 2345–2348.

Wang, Y.J., et al., 2005. The holocene asian monsoon: links to solar changes and North Atlantic climate. Science 308 (5723), 854–857.

Wang, Y.J., et al., 2008. Millennial- and orbital-scale changes in the East Asian monsoon over the past 224,000 years. Nature 451 (7182), 1090–1093.

Wu, K., Shen, L., Zhang, T., Xiao, Q., Wang, A., 2015. Links between host rock, water, and speleothems of Xueyu Cave in Southwestern China: lithology, hydrochemistry, and carbonate geochemistry. Arab. J. Geosci. 8 (11), 8999–9013.

Wu, Y., Xu, Y., Li, H., Xing, D., 2012. Effect of acetazolamide on stable carbon isotope fractionation in *Chlamydomonas reinhardtii* and *Chlorella vulgaris*. Chin. Sci. Bull. 57 (7), 786–789.

Xie, T., Wu, Y., 2014. Can carbon in calcium carbonate be utilized by microalgae. Earth Environ. 42 (02), 168–173 (in Chinese).

Xu, Q., et al., 2017. *Arthrobacter* sp. strain MF-2 induces high-Mg calcite formation: mechanism and implications for carbon fixation. Geomicrobiol. J. 34 (2), 157–165.

Yuan, D., et al., 2004. Timing, duration, and transitions of the Last Interglacial Asian Monsoon. Science 304 (5670), 575–578.

Zhang, H., et al., 2018. East Asian hydroclimate modulated by the position of the westerlies during Termination I. Science 362 (6414), 580–583.

Zhou, G., Guan, Y., Yao, Q., Fu, S., 2010a. Biomimetic mineralization of prismatic calcite mesocrystals: relevance to biomineralization. Chem. Geol. 279 (3–4), 63–72.

Zhou, X., Du, Y., Lian, B., 2010b. Effect of different culture conditions on carbonic anhydrase from *Bacillus mucilaginosus* inducing calcium carbonate crystal formation. Acta Microbiol. Sin. 50 (7), 955–961 (in Chinese).

Zhuang, D., et al., 2018. Calcite precipitation induced by *Bacillus cereus* MRR2 cultured at different Ca^{2+} concentrations: further insights into biotic and abiotic calcite. Chem. Geol. 500, 64–87.